Journal of Physics: Conference Series

PAPER • **OPEN ACCESS**

Photocatalytic degradation of rhodamine B dye under visible light using cerium-cobalt co-doped bismuth ferrite nanoparticles

To cite this article: N Jamaludin *et al* 2023 *J. Phys.: Conf. Ser.* **2432** 012015

Photocatalytic degradation of rhodamine B dye under visible light using cerium-cobalt co-doped bismuth ferrite nanoparticles

N Jamaludin[1], N A A Razak[2], F D Ismail[2], and K T Chaudhary[3]

[1] Laser Center, Ibnu Sina Institute for Scientific and Industrial Research, Universiti Teknologi Malaysia, 81310 Skudai, Johor, Malaysia
[2] Department of Physics, Faculty of Science, Universiti Teknologi Malaysia, 81310 Skudai, Johor, Malaysia
[3] Department of Physics, COMSATS University Islamabad, Lahore Campus, Raiwind Road, Lahore, Pakistan

Email: nazihajamaludin91@gmail.com

Abstract. The present study designates the photocatalytic degradation efficiency of RhB dye using cerium-cobalt co-doped $BiFeO_3$ nanoparticles. Nanoparticles of $Ce_{0.1}Co_xBi_{1-x}Fe_2O_3$ ($0 \leq x \leq 0.2$) have been facilely synthesized via sol-gel auto-combustion method. FESEM analysis revealed the irregular-shaped nanoparticles with agglomerated coalescence behaviour and the element composition in $Ce_{0.1}Co_xBi_{1-x}Fe_2O_3$ ($0 \leq x \leq 0.2$) was confirmed in EDX. The crystallite size can be calculated around 64 nm to 71 nm for pure $BiFeO_3$ nanoparticles and in range of 41 nm to 60 nm for the co-doped $BiFeO_3$ nanoparticles. XRD diffraction confirmed the presence of secondary phase (Sillenite) and tertiary phase (Millate) when dopant concentration increased. From TGA profile, the ideal annealing temperature of 600 °C have been confirmed for all samples. Furthermore, the photocatalytic degradation of RhB dye has been improved via cerium-cobalt co-doping. UV spectra showed that the RhB dye solution constantly changes pink colour into colourless within 20 minutes of visible light irradiation to fully degraded.

1. Introduction

The rapid industrial development and urbanization has greatly contributed to the increase in water pollution. The textile industry is one of the most chemically intensive industries which discharges a significant amount chemical pollutants from the processes of dyeing and finishing [1, 2]. The consumption of contaminated water with dyes from the textile industry have very adverse effect on the human body and aquatic life even at very low concentration as 1.0 mg/l [3]. There are several types of textile dyes including anionic (acid, direct and reactive dyes), cationic dyes (basic dyes) and non-ionic (disperse dyes) are used for dying process. Rhodamine B (RhB) is a typical and highly water-soluble dye, widely used in the industry [4]. The contamination of water by RhB can lead to undesired consequences to human beings and the environment [5]. Rhodamine B (RhB) is toxic and carcinogenic, causing allergy and skin irritation [6, 7].

Water pollution caused by dyes is a global concern as the water treatment through cost-effective and eco-friendly techniques is a challenging task. The contaminated water requires proper treatment before discharge to the environment to avoid the toxic effect. Numerous treatment methods that including coagulation, reverse osmosis, filtration, ozonisation, membrane filtration, adsorption, ion exchange, and photodegradation have been used for the chemically contaminated wastewater. Among available physical methods, photodegradation is one of the excellent methods to remove dyes contents from wastewater with effectiveness and simplicity [8].

Photocatalysis is a technique that use to modify the rate of chemical reaction with the presence of light to activate the catalyst substance without being involved itself. This technique is used for the reduction of organic pollutants in water such as rhodamine B, methyl orange and many more organic dyes that are normally used in textile, dyeing, printing, and cosmetic industries. The presence of visible light also influenced the photocatalytic efficiency in photodegradation of dyes. The previous study shown that the photocatalytic process can be activated with a photon transition under the irradiation of visible light [9]. This presence of light results in the modification of photoreaction rate as it involves the absorption of light that initiated the photoexcitation of semiconductor due to the transition of electron from ground state to excited state forming the positive and negative charges on nanocomposite energy levels and based on the structure and ability of the catalyst to create the electron-hole pairs. These electron-hole pairs can generate the free radicals such as hydroxyl radicals which can help the secondary reaction either oxidation or reduction reaction to take place.

A diverse class of magnetic nanoparticles includes ferrite nanoparticles. The ferrite nanoparticles are known as metal oxides with spinel structure. The general formula of the ferrite nanoparticles is AB_2O_4 [10]. The metallic cations (A and B in the general formula) are located at two different types of crystallographic sites known as octahedral and tetrahedral sites. The cations at both of the sites are coordinated with oxygen atoms [11]. To be referred to as "ferrite," the chemical compound iron (III) must be present in the formula. For example, MFe_2O_4, where M is a metal. These particles could be having the properties of superparamagnetic with the size around 20 nm and below. Based on their affinity for both orientations, the metal cations are allocated to the tetrahedral and octahedral sites. The distribution of the cations can have a significant impact on the chemical and physical properties of ferrite nanoparticles [12]. Ferrites are classified according to their magnetic properties and the crystal structure. Few types of ferrites are spinel, garnet and ortho ferrite while some examples of the crystal structures are cubic, perovskite and hexagonal [13].

$BiFeO_3$ is acknowledged as multiferroic material as $BiFeO_3$ have simultaneously magnetic and electric ordering. Recently, due to its low band gap and strong bulk photovoltaic effect, $BiFeO_3$ has recently drawn a lot of interest in solar applications. Instead of solar application, due to its small band gap of 2.1–2.7 eV, BiFeO3 is capable of performing photocatalytic activity under visible light [14]. This is important to perform photocatalytic activity under visible light as UV supplies to only 4% of solar radiation, while visible light supplies to about 50% of solar radiation [15]. Furthermore, since $BiFeO_3$ is a ferroelectric material, it has many interesting features such as charge-carrier separation in a homogenous medium, and a photocurrent proportional to the polarization magnitude [14]. The depolarization of electric field presence in $BiFeO_3$ can decrease the recombination of the photogenerated charged carriers during the transmission process [16]. Throughout this process, the quantum efficiency can be increased. Hence, $BiFeO_3$ can act as a promising photocatalyst for degradation of organic pollutants [17].

Recently, most researchers used noble metals to improve the photocatalytic performance of the materials. In this study, the cost-effective photocatalytic degradation method is used to degrade RhB dye by using $BiFeO_3$ nanoparticles as photocatalysts because they have shown a great potential for

photodegradation of dyes when doped with metal cations as it enhances the photocatalytic activity. Photodegradation of dyes with $BiFeO_3$ containing dopant was found to be 2.7 times higher than pure BFO materials [18]. Degradation of dyes are also affected by pH condition of the dyes itself. From previous research, it was found that the highest photocatalytic activity is under acidic condition for RhB dye. The $BiFeO_3$ nanoparticles especially with insertion of dopant can enhance the properties of photocatalytic activity for degradation of organic dyes to be applied in water treatment process. Then, both doped and undoped ferrites have gained a great interest in catalysis, and for this study, undoped $BiFeO_3$, Cerium-doped $BiFeO_3$ and Cerium-Cobalt co-doped $BiFeO_3$ were synthesized, characterized, and analysed for the photocatalytic degradation of RhB dye. Several parameters affecting the catalytic activity were also optimized.

2. Experimental methods

2.1. Materials

Cerium (III) chloride heptahydrate ($CeCl_3.7H_2O$); Cobalt (II) nitrate hexahydrate ($Co(NO_3)_3.6H_2O$); bismuth (III) nitrate pentahydrate ($Bi(NO_3)_3.5H_2O$); citric acid monohydrate ($C_6H_8O_7.H_2O$); iron (III) nitrate nonahydrate ($Fe(NO_3)_3.9H_2O$); nitric acid (HNO_3); rhodamine B dye ($C_{28}H_{31}ClN_2O_3$); hydrochloric acid (HCl); and hydrogen peroxide (H_2O_2) of AR grade were applied as such without additional purification for preparing samples.

2.2. Synthesis of cerium and cobalt co-doped $BiFeO_3$ nanoparticles

The $Ce_{0.1}Co_xBi_{1-x}Fe_2O_3$ ($0 \leq x \leq 0.2$) nanoparticles were grown through the sol-gel auto-combustion (SAC) method. Firstly, bismuth (III) nitrate pentahydrate, iron (III) nitrate nonahydrate and dilute nitric acid were used as starting materials. The bismuth nitrate and iron nitrate were dissolved in diluted nitric acid in proportion of 1:1 (molar ratio) with 0.1M respectively. Each solution was stirred and heated on the hotplate at 80°C for 10 minutes until the solutions homogeneously dissolved. Citric acid was used as the chelating agent for sol-gel auto combustion process. Afterward, both of metal nitrates solutions were mixed and stirred at 80°C for another 10 minutes, followed by adding the citric acid into the solution, and then heated up to 300 ºC until combustion occurred. The resultant flakes were collected, dried in an oven for one hour at 200˚, grounded and annealed in a furnace for 4 h at 600 ºC with heating rate of 5℃/min.

2.3. Photocatalytic Degradation of Rhodamine B

The photocatalytic degradation of RhB dye solution was investigated by using synthesized $BiFeO_3$ with different dopant concentration ($Ce_{0.1}Co_xBi_{1-x}Fe_2O_3$, where $0 \leq x \leq 0.2$). A photocatalytic reactor with reflective surface inside was designated to received maximum absorption of light is demonstrated in Figure 1. A 150 W metal halide lamp was used as visible light source for the photocatalytic activity. RhB dye stock solution was prepared by dissolving and stirring 10 mg RhB dye into 1 L of deionized water. The RhB dye solution was adjusted and maintained at pH 2 by dropping HCl. 80 mg of the synthesized $Ce_{0.1}Co_xBi_{1-x}Fe_2O_3$ ($0 \leq x \leq 0.2$) photocatalyst was evenly distributed into 100 ml of RhB dye solution. 1 ml of H_2O_2 was added as booster to speed up the reaction as it could generate more OH-radicals during degradation process. At the beginning, the prepared solution was kept under dark inside the photoreactor at room temperature and stirred for 30 minutes by using magnetic stirrer before irradiating it with visible light. This will enable the $Ce_{0.1}Co_xBi_{1-x}Fe_2O_3$ ($0 \leq x \leq 0.2$) nanoparticles and RhB dye solution to achieve equilibrium adsorption condition. After that, the lamp was switched on and 10 ml of the dye solution was drawn with 5 minutes interval for 30 minutes for further samples.

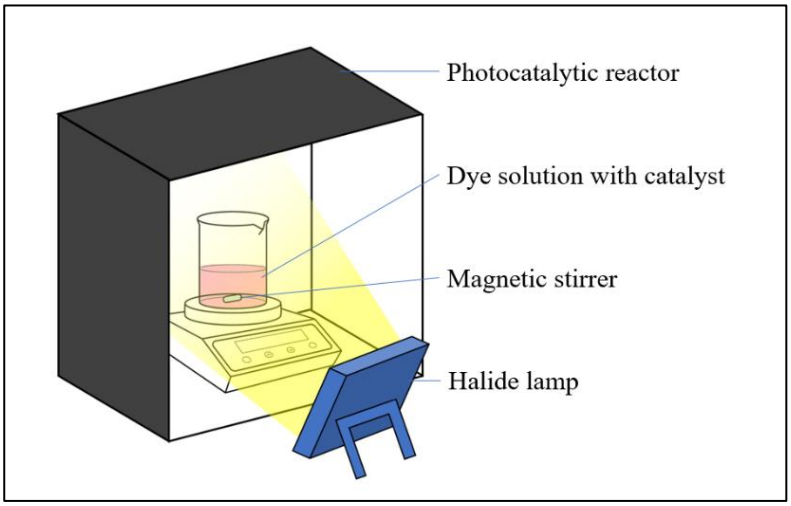

Figure 1. Schematic of the photocatalytic reactor setup.

2.4. Characterization

The thermal decomposition profile of pure and doped $BiFeO_3$ nanoparticle catalysts were determined by Thermogravimetric analysis (TGA) to find the appropriate temperature range for annealing. The powder of $BiFeO_3$ exposed to heat at range temperature of 25 ℃ to 1000 ℃ with ramping temperature of 1℃/min. Surface morphologies and size of nanoparticles were determined by using Field Emission Scanning Electron Microscope (FESEM) and Energy Dispersive X-ray (EDX). X-ray Diffractometer (XRD) served to determine the phases and crystallinity of the synthesized nano ferrite samples over a 2θ range to 10^o to 80^o. UV-Visible spectroscopy was used to identify the chemical structure and absorption of Rhodamine B (RhB) dye solution before and after the degradation at different time.

3. Results and Discussion

3.1. Thermogravimetric (TGA) Analysis

Figure 2(a) shows the simultaneous TG-DTA plot of $BiFeO_3$ nanoparticles synthesized using sol-gel auto combustion method using citric acid as a fuel. The x-axis presents the temperature variation while y-axis is the concentration weight loss of the $BiFeO_3$ (black line) and first derivative curve (red line). From the curve, a small weight loss is observed around 70 ℃ to 150℃ which attributes to the decomposition of water content [19] . Exothermic peaks are observed around 273℃ and 327°℃ for temperature range 250℃ to 375℃. The decrements might be due to the decomposition of $NO3-$ ions, side chain of O-H and C-H group and the loss of COO group of citric acid fuel [20]. After 375°C, the degrees gradually decreasing up to 750°C due to instability of BFO rhombohedral structure and the decrement at 827°C and 973°C associated to rhombohedra to orthorhombic structural phase transition [21] . From the temperature 500°C to 937°C shown in DTA line, no further decrease in weight which indicates the stabilization of crystallization of perovskite crystal structure. This temperature range is the ideal annealing temperature rang [22].

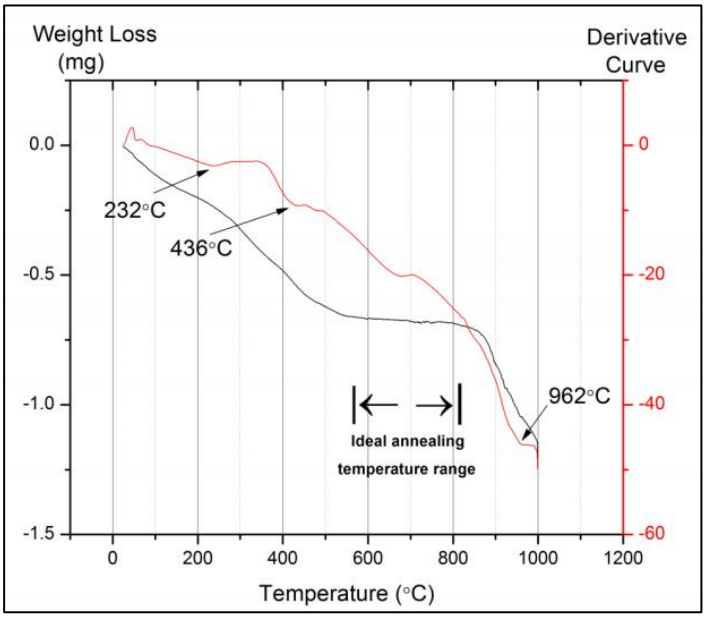

Figure 2(b). TGA-DTA profile of cerium-doped $BiFeO_3$ nanoparticles.

Figure 2(b) shows the TGA-DTA profile of Cerium-doped $BiFeO_3$ nanoparticles. The graph shows a small weight loss in temperature range 70°C to 150°C is noticed due to the loss of water molecules which added during the fabrication process [19]. A significant weight loss as shown in DTA graph is perceived at temperature of 436°C caused by the decomposition of metal nitrates anion and organic residue [20]. A plateau region around temperature 530°C to 820°C where no significant change in thermal decomposition and this temperature range suitable for annealing process of nanoparticles [21]. From the TGA profile, 600°C is chosen as the ideal annealing temperature of all the samples of $BiFeO_3$ nanoparticles as the material has achieved stabilization stage of perovskite crystal structure [22].

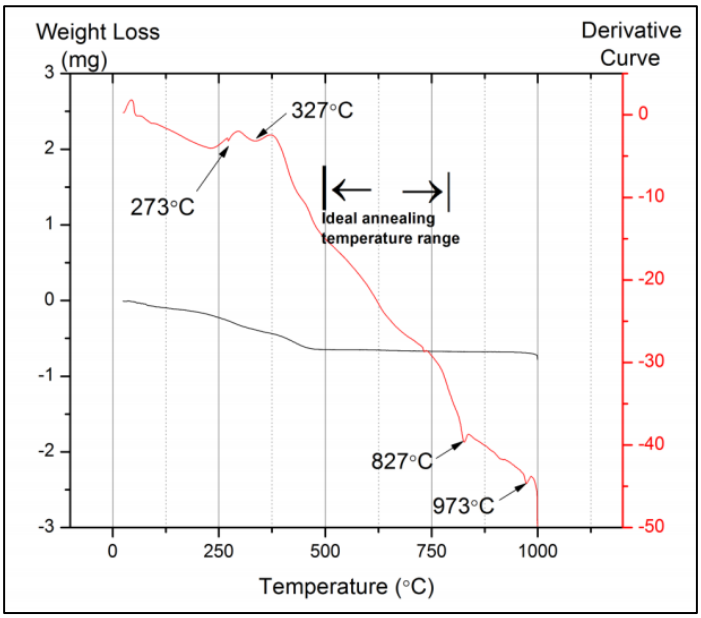

Figure 2(a). TGA profile of $BiFeO_3$ nanoparticles.

3.2. Field Emission Scanning Electron Microscope (FESEM) Analysis

Figure 3(a-f) illustrate the surface morphology of the $BiFeO_3$ with different dopant concentration ($Ce_{0.1}Co_xBi_{1-x}Fe_2O_3$, where $0 \leq x \leq 0.2$). FESEM images show the irregular shaped particles with agglomeration behaviour. This behaviour exists due to the change of the magnetic properties [23]. The agglomerate size will increase if the particle size as the ratio of surface to volume is increase. From Figure 3(a-f), the average size calculated for the particle are 64.52 nm, 50.58 nm, 52.45 nm, 59.69 nm, 60.67 nm, and 53.75 nm, respectively. The average size calculated for all samples are almost the same with the crystalline size that determined from XRD analysis.

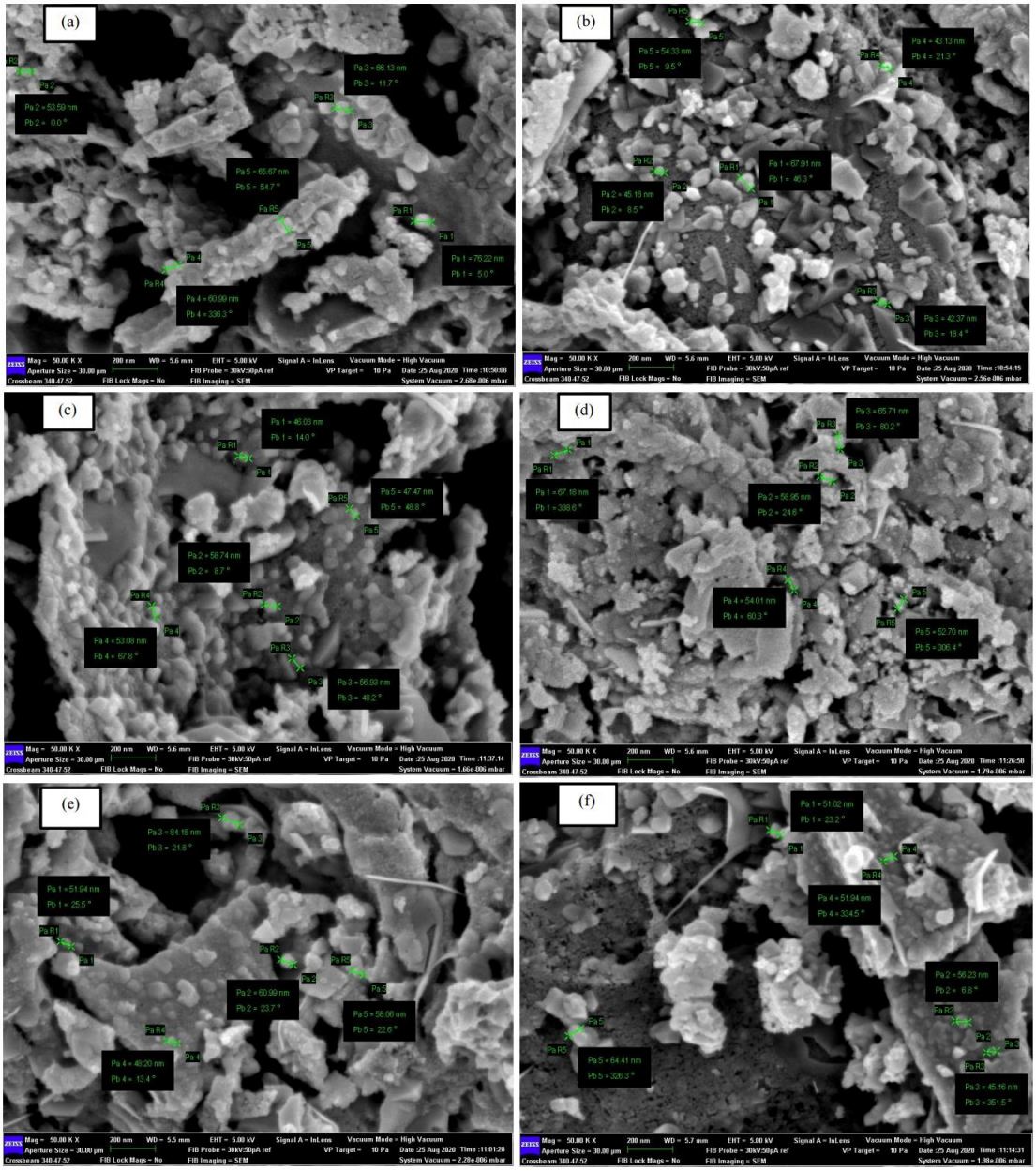

Figure 3. FESEM micrographs of synthesized $BiFeO_3$ nanoparticles with different dopant concentration, $Ce_{0.1}Co_xBi_{1-x}Fe_2O_3$, where x = **(a)** (undoped), **(b)** 0%, **(c)** 5%, **(d)** 10 %, **(e)** 15% and **(f)** 20%.

3.3. Energy Dispersive X-ray (EDX) Analysis

Figure 4 displays the EDX spectra of synthesized $Ce_{0.1}Co_xBi_{1-x}Fe_2O_3$ ($0 \leq x \leq 0.2$) nanoparticles. Overall, the spectra confirm the presence of bismuth (Bi), cerium (Ce), iron (Fe) and Oxygen. All elements are well distributed throughout the region. The existence of this unwanted compound might be due to the citric acid that used as a fuel during the fabrication process.

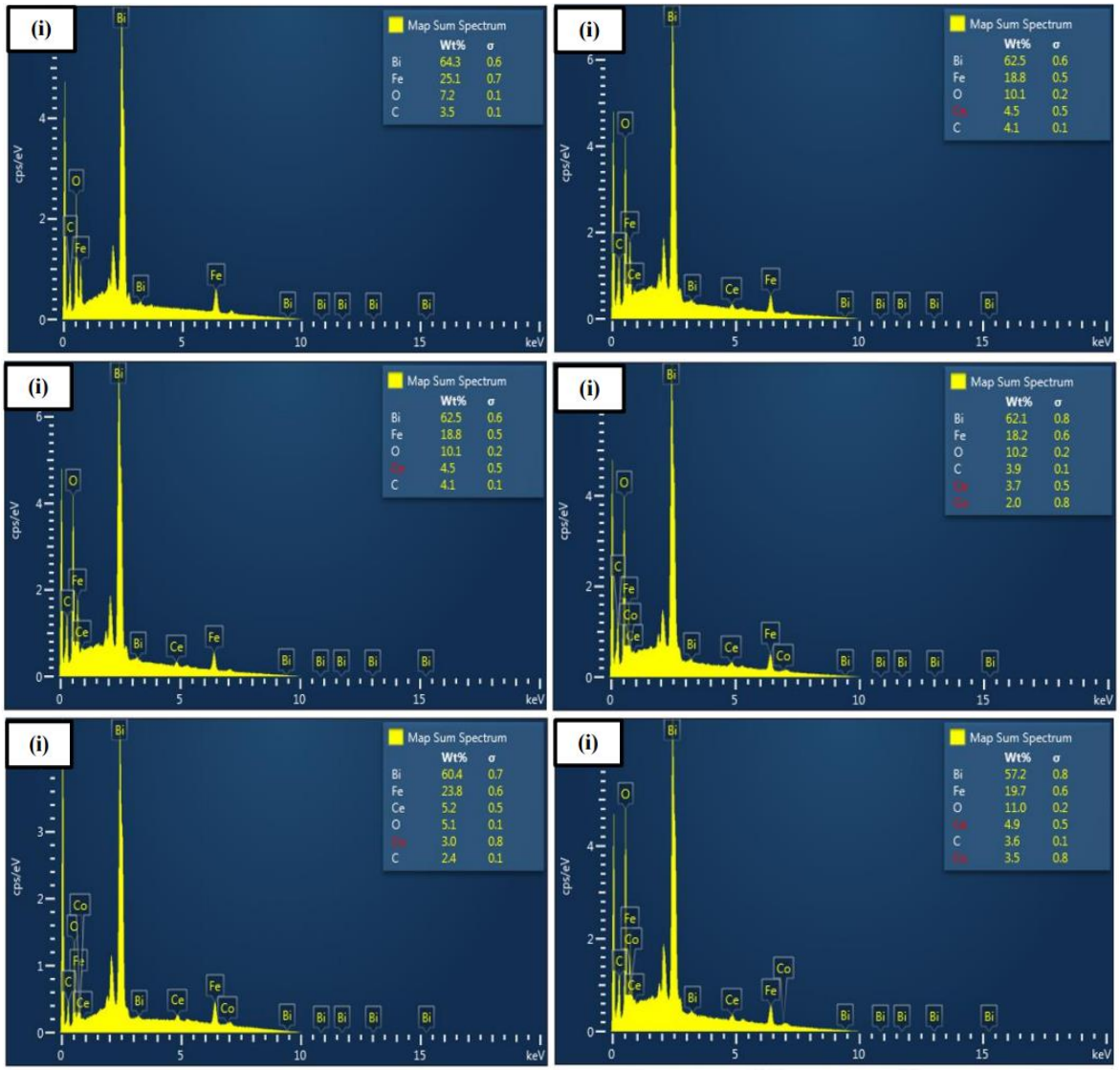

Figure 4. EDX spectra of synthesized $BiFeO_3$ nanoparticles with different dopant concentration, $Ce_{0.1}Co_xBi_{1-x}Fe_2O_3$, where x = **(a)** (undoped), **(b)** 0%, **(c)** 5%, **(d)** 10 %, **(e)** 15% and **(f)** 20%.

From all spectra, the EDX results obtained are almost the same. The presence of Bi, Fe, O and Co elements is confirmed in samples before and after the photocatalytic degradation of RhB dye. It is found out that there is no change in the phase of the nanoparticles even after the photocatalytic degradation of RhB dye.

3.4. X-Ray Diffraction (XRD) Analysis

Figure 5 shows the XRD spectra for synthesized $BiFeO_3$ with different dopant concentration ($Ce_{0.1}Co_xBi_{1-x}Fe_2O_3$ where $0 \leq x \leq 0.2$). In XRD spectra, three different phases are observed which were Bismuth ferrite ($BiFeO_3$) hexagonal structure, Sillenite ($Bi_{25}FeO_{40}$) cubic structure and Millate $Bi_2Fe_4O_9$ orthorhombic structure based on R3c space group, 123 group and Pbam space group respectively. The plane that associated to $BiFeO_3$ (bismuth ferrite) hexagonal structure are (012), (104), (110), (202), (024), (116), (214), 29 (220), (306) and (134) where $Bi_{25}FeO_{39}$ (sillenite) cubic structure are (301), (222) and (440). For $Bi_2Fe_4O_9$ (millate) orthorhombic structure, the associated planes are (112), (430), (204) and (230). The spectra shows that the R3c space group dominated the structure. And some of the peaks starts to disappear as the doping introduced.

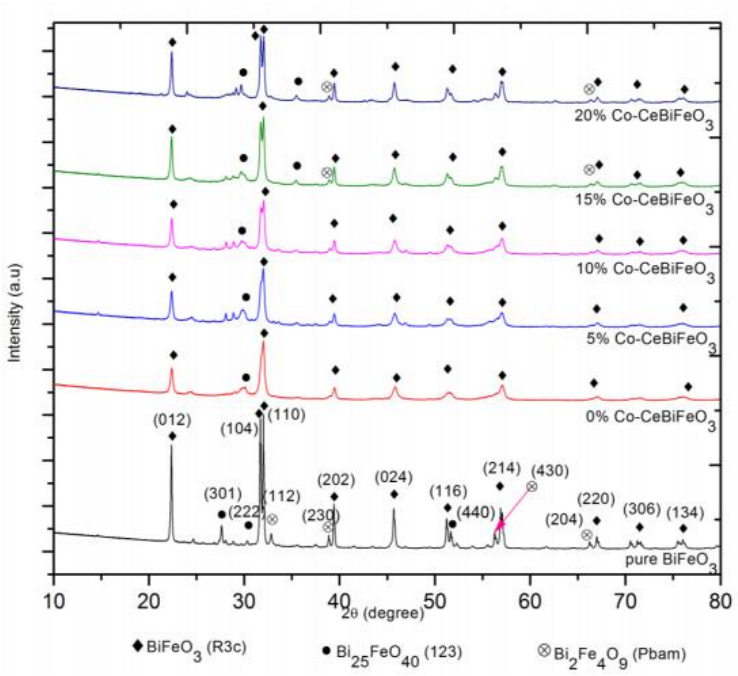

Figure 5. XRD spectrum of synthesized $BiFeO_3$ with different dopant concentration, $Ce_{0.1}Co_xBi_{1-x}Fe_2O_3$, where x = undoped, 0%, 5%, 10 %, 15% and 20%.

Figure 6 shows the zoomed-in spectral lines at region 31.4° to 32.4° with plane (104) and (110) linked to hexagonal structure. The adding of doping into the pure $BiFeO_3$ gives a significant change in the line profile of the XRD pattern. As only cerium doped into pure $BiFeO_3$ (zero concentration of cobalt), the (104) and (110) peaks get broadened resemble a single peak. This situation is due to the difference in the electron density of the cerium atom or the cerium atom substitute into the $BiFeO_3$ lattice and structural distortion of hexagonal structure of bismuth ferrite. However, the peak become narrower and split into two peaks again with the increasing of doping (cobalt) concentration as the cobalt is introduced. The introduction of the cobalt to the undoped $BiFeO_3$ nanoparticles caused structural distortion in crystal structure [24].

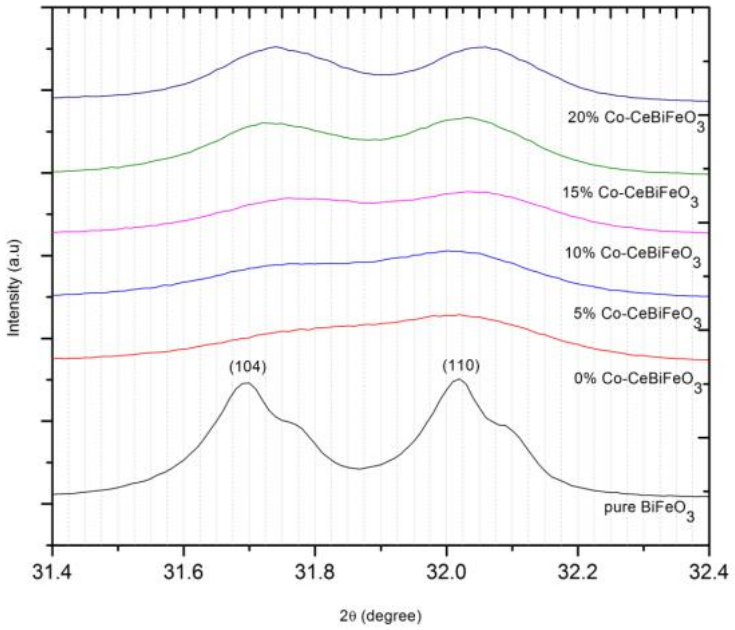

Figure 6. Broaden peaks of (104) and (110) plane of undoped $BiFeO_3$ and $Co_xCeBi_{1-x}FeO_3$ nanoparticles with different concentration of cobalt (x=0, 0.05, 0.10 and 0.20).

The crystallize size of synthesized $BiFeO_3$ is determined by Debye-Scherrer's equation (1) as given below [25]:

$$D = \frac{0.9\lambda}{\beta cos\theta} \quad (1)$$

Where D is crystalline size, λ is wavelength of the X-ray, β is the full width half maximum (FWHM) and θ is Bragg diffraction angle. All the calculation parameters are selected from the most intense peak of XRD spectra, applied for all samples. The crystallite size of undoped $BiFeO_3$ nanoparticles is 71.80 nm while for $Ce_{0.1}Co_xBi_{1-x}Fe_2O_4$ nanoparticles with different concentration of x=0, 0.05, 0.10, 0.15 and 0.20 are 41.9 nm, 50.60 nm, 55.19 nm, 56.71 nm, and 60.14 nm, respectively.

The crystallite size of doped $BiFeO_3$ at with the presence of cerium only (where x = 0) shows the smallest crystallite size compared to all samples. The changes of crystallite size might be due to the disappearance of bismuth ferrite ($BiFeO_3$) phase. However, when the concentration increased from x= 0.05 to x = 0.20, the size of crystallite started to increase. Since the atomic radius of Co^{2+} (1.88Å) and Fe^{3+}(1.90Å) are comparable, this may lead to replacement of B-site of $BiFeO_3$ with transitional metal (Co) ion. Due to the slight variation in the atomic radius, the compressive strain is generated in the matrix, which causes the slight variation in crystallite size in cobalt doped $BiFeO_3$ nanoparticle [26].

Figure 7 shows the crystalline size of $Ce_{0.1}Co_xBi_{1-x}Fe_2O_4$ nanoparticles with different concentration of cobalt (x=0, 0.05, 0.10, 0.15 and 0.20) in the range of 40 nm to 60 nm. The graph illustrated that the crystallite size increased as the dopant (cobalt) concentration increased. The increase of crystallite size might be due to the surface distortion as high amount of cobalt is introduced into the host as a dopant. The increase in the crystallite size might be due to the greater amount of distortion as the cobalt doping concentrations are high in amount [27].

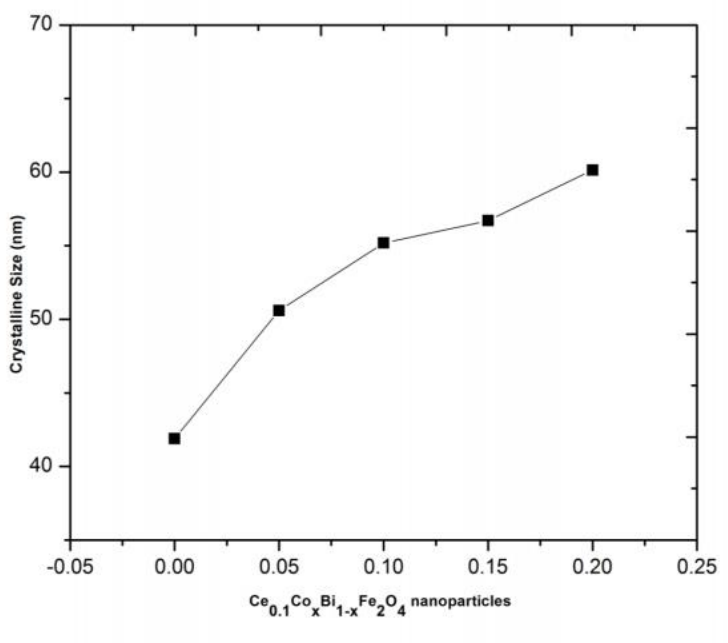

Figure 7. Crystalline size of $Ce_{0.1}Co_xBi_{1-x}Fe_2O_4$ nanoparticles with different concentration of cobalt (x=0, 0.05, 0.10, 0.15 and 0.20).

3.5. UV-Visible Analysis for Photocatalytic Degradation of Rhodamine B Dye

Photocatalytic degradation of Rhodamine B (RhB) dyes is performed under the exposure of visible light in the span of 30 minutes. The undoped $BiFeO_3$ and co-doped $BiFeO_3$ nanoparticles are examined to study their ability to degrade RhB dyes. The co-doped composites had the formula $Ce_{0.1}Co_xBi_{1-x}Fe_2O_4$ where x = 0.05, 0.10, 0.15 and 0.20. The degradation of RhB dye over time is determined by UV-Vis spectrometer.

Figure 8(a-f) shows the UV-Visible spectra that recorded the absorbance of RhB at different times of degradation process for a span of 30 minutes using undoped bismuth ferrite ($BiFeO_3$) and Cerium-Cobalt bismuth ferrite ($Ce_{0.1}Co_xBi_{1-x}Fe_2O_4$) nanoparticles with different Cobalt concentration (x = 0.0, 0.05, 0.10, 0.15, 0.20). Firstly, the photocatalytic degradation of RhB solution is tested by using undoped (pure) $BiFeO_3$ nanoparticles as shown in Figure 8(a). From the result obtained, RhB solution have fully degraded at 30 minutes under exposure of visible light. In the case of doped $BiFeO_3$ with zero concentration of cobalt which means only the presence of cerium as a dopant, the rate of photocatalytic degradation improved significantly as RhB dye are completely degraded at 20 minutes of irradiation time as illustrated in Figure 8(b).

The concentrations of dopant are varied at x = 0.05 ($Ce_{0.1}Co_{0.05}Bi_{0.9}Fe_2O_4$), x = 0.10 ($Ce_{0.1}Co_{0.1}Bi_{0.9}Fe_2O_4$), x = 0.15 ($Ce_{0.1}Co_{0.15}Bi_{0.85}Fe_2O_4$), and x = 0.20 ($Ce_{0.1}Co_{0.2}Bi_{0.8}Fe_2O_4$), as presented in Figure 8 at (c), (d), (e) and (f), respectively. At concentration of x = 0.05 shown in Figure 8(c), RhB dye seemed to fully degrade at 30 minutes of irradiation whereas for x = 0.10 in Figure 8(d), the rate of photocatalytic degradation increased as RhB solution only took 20 minutes to undergo a complete degradation. As the concentration increased from x = 0.15 to x = 0.20, the photodegradation rate become a bit slower compared to x = 0.10 as both samples have completely degraded after 20 minutes under irradiation of visible light. The samples of RhB dye solutions are collected after 5 minutes intervals for 30 minutes during photocatalytic process. The RhB solution constantly changes colour from bright pink to light pink and then turns into a colourless solution. The colour changes due to the breakdown of the chromophoric group that existed in the solution [28].

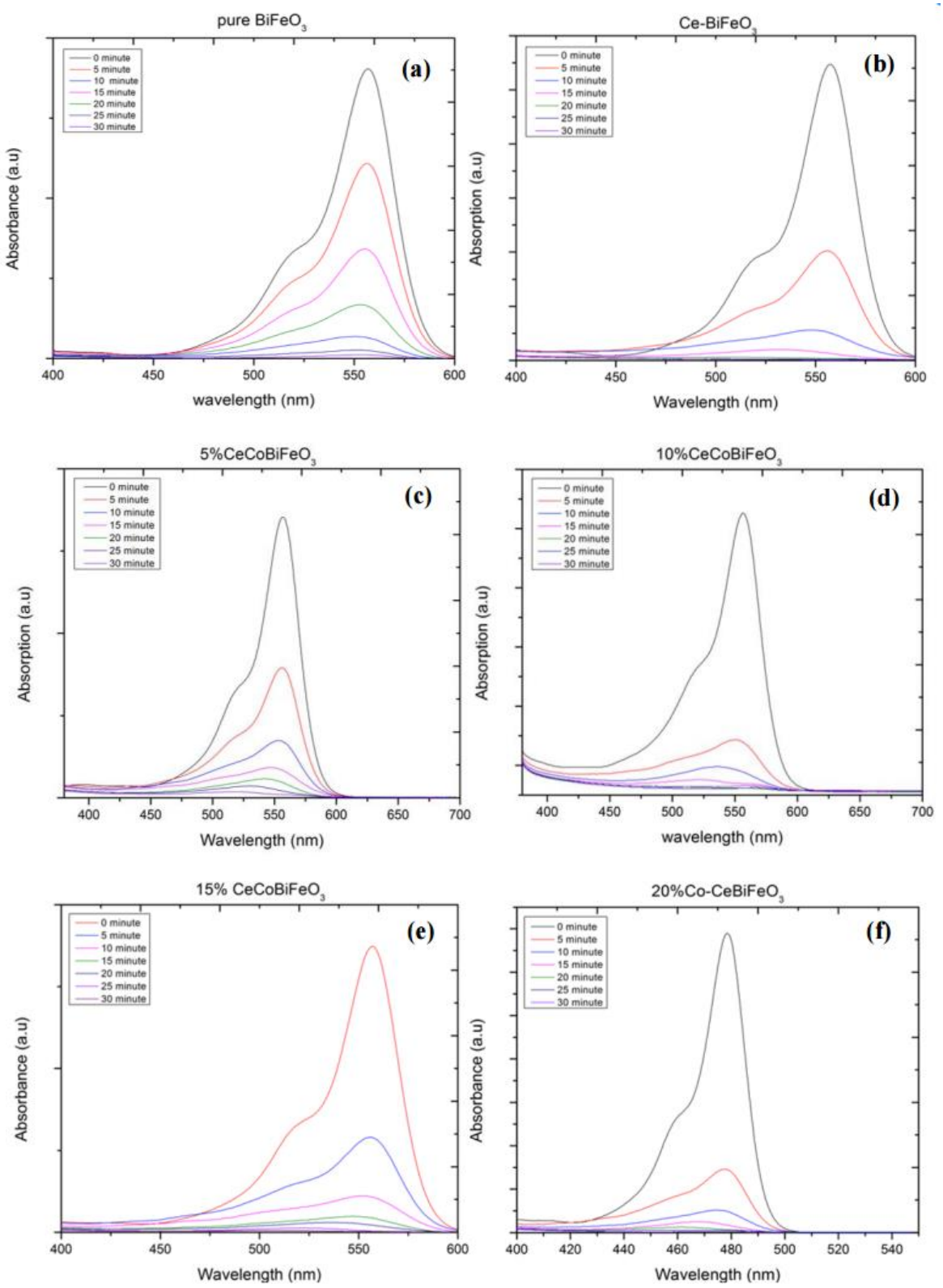

Figure 8. UV-Visible spectra of photocatalytic degradation of RhB using **(a)** undoped $BiFeO_3$, and doped $BiFeO_3$ with different doping concentration, x ($Ce_{0.1}Co_xBi_{1-x}Fe_2O_4$) **(b)** x = 0.0, **(c)** 0.05, **(d)** 0.10, **(e)** 0.15 and **(f)** 0.20

Furthermore, the peak wavelengths have shifted as shown in Figure 8(f). This is because of the de-ethylation and discolouration of RhB due to the presence of Co^{2+}ions [29] in $Ce_{0.1}Co_{0.2}Bi_{0.8}Fe_2O_4$ nanoparticles as the concentration 0.20 of cobalt is enough to show a clear change in peak wavelength. Overall, the most efficient photocatalysis degradation of RhB solution take place when there are zero concentration of cobalt (x = 0) which means there only cerium that acted as a dopant in this sample as it only takes 20 minutes of visible light irradiation to fully degraded. From the UV-Vis analysis, the obtained spectra proved that the presence of Co^{2+} ions in the bismuth ferrite nanoparticles delay the degradation process as the existence of them slow up the recombination process of the electron-hole pair [30].

4. Conclusion

The nanoparticles size gives a big impact for degradation of RhB dye solution as they act as photocatalyst because the smaller the size, the rate of photocatalytic activity increased due to the ration of surface to volume is increased. Among the synthesized nanoparticles, $Ce_{0.1}Co_xBi_{1-x}Fe_2O_4$ where dopant concentration x = 0.0 (no presence of cobalt) presented as the best photocatalyst for degradation of RhB solution. Overall, all samples of cerium-cobalt co-doped bismuth ferrite nanoparticles were successfully synthesized, and their structural and optical properties were improved as compared to pure bismuth ferrite.

5. References

[1] Kant R 2011. Textile dyeing industry an environmental hazard. Malik, R., Ramteke, D. S., & Wate, S. R. (2007). Adsorption of malachite green on groundnut shell waste based powdered activated carbon. *Waste management* **27(9)** 1129-1138

[2] Gupta V K, Carrott P J M, Carrott M M L R, and Suhas 2009. Low-cost adsorbents: growing approach to wastewater treatment-a review. *Crit Rev Environ Sci Technol* **39(10)** 783-842

[3] Tariq M, Muhammad M, Khan J, Raziq A, Uddin M K, Niaz A, and Rahim A 2020. Removal of Rhodamine B dye from aqueous solutions using photo Fenton processes and novel Ni-Cu@ MWCNTs photocatalyst. *Journal of Molecular Liquids* 113399

[4] Wang M, Fu J, Zhang Y, Chen Z, Wang M, Zhu J, and Xu Q 2015. Removal of Rhodamine B, a cationic dye from aqueous solution using poly (cyclotriphosphazene-co-4, 4′-sulfonyldiphenol) nanotubes. *Journal of Macromolecular Science* A **52(2)** 105-113

[5] Lima E C, Royer B, Vaghetti J C, Simon N M, da Cunha B M, Pavan F A, and Airoldi C 2008. Application of Brazilian pine-fruit shell as a biosorbent to removal of reactive red 194 textile dye from aqueous solution: kinetics and equilibrium study. *Journal of hazardous materials* **155(3)** 536-550

[6] Huang M, Wang L, Zhang K, Yan M, Li Y, Zhu Z, and Yang J 2020. Preparation of three-dimensional flower-like Fe-Bi (OH) 3 nanocomposites and the photocatalytic properties for degradation of Rhodamine B in presence of visible light. *Optik* 164876

[7] Ghafuri H, Dehghani M, Rashidizadeh A, and Rabbani M 2019. Synthesis and characterization of magnetic nanocomposite Fe_3O_4@ TiO_2/Ag, Cu and investigation of photocatalytic activity by degradation of rhodamine B (RhB) under visible light irradiation. *Optik* **179** 646-653

[8] Reddy B P, Sekhar M C, Prakash B P, Suh Y, and Park S H 2018. Photocatalytic, magnetic, and electrochemical properties of La doped $BiFeO_3$ nanoparticles. *Ceramics International* **44(16)** 19512-19521

[9] Wang K, Xu J, Hua X, Li N, Chen M, Teng F, and Yao W 2014. Highly efficient photodegradation of RhB–MO mixture dye wastewater by Ag_3PO_4 dodecahedrons under acidic condition. *Journal of Molecular Catalysis A: Chemical* **393** 302-308

[10] Wu W, Wu Z, Yu T, Jiang C, and Kim W-S 2015. Recent progress on magnetic iron oxide nanoparticles: synthesis, surface functional strategies and biomedical applications. *Science*

and technology of advanced materials **16(2)** 023501-023501
[11] Hill R J, Craig J R, and Gibbs G V 1979. Systematics of the spinel structure type. *Physics and Chemistry of Minerals* **4(4)** 317-339
[12] Tian R, Yang G, Zhu C, Liu X, and Li H 2015. Specific Anion Effects for Aggregation of Colloidal Minerals: A Joint Experimental and Theoretical Study. *The Journal of Physical Chemistry ,* **119(9)** 4856-4864
[13] Liou J G, Tsujimori T, Yang J, Zhang R Y, and Ernst W G 2014. Recycling of crustal materials through study of ultrahigh-pressure minerals in collisional orogens, ophiolites, and mantle xenoliths: A review. *Journal of Asian Earth Science,* **96** 386-420
[14] Sharma K, and Singh A 2016. Journal of Nanoscience and Technology. *Journal of Nanoscience and Technology* **2(2)** 85-90
[15] Jafari T, Moharreri E, Amin A S, Miao R, Song W, and Suib S L 2016. Photocatalytic water splitting-the untamed dream: a review of recent advances. *Molecules* **21(7)** 900
[16] Idriss H, Nadeem M, and Khan M 2016. Ferroelectric polarization effect on surface chemistry and photo-catalytic activity: A review. *Surface Science Report* **71(1)** 1-31
[17] Kanhere P, and Chen Z 2014. A review on visible light active perovskite-based photocatalysts. *Molecules* **19(12)** 19995-20022
[18] Favela-Camacho S E, Samaniego-Benítez E J, Godínez-García A, Avilés-Arellano L M, and Pérez-Robles J F 2019. How To Decrease The Agglomeration Of Magnetite Nanoparticles And Increase Their Stability Using Surface Properties. *Colloids And Surfaces A: Physicochemical And Engineering Aspects* **574** 29-35
[19] Sakar M, Balakumar S, Saravanan P, and Jaisankar S N 2016. Electric field induced formation of one-dimensional bismuth ferrite ($BiFeO_3$) nanostructures in electrospinning process. *Materials & Design* **94** 487-495
[20] Ashok A, Kumar A, Bhosale R, Saad M, and Jp van den Broeke L 2015. *Cellulose Assisted Combustion Synthesis of Porous Cu-Ni Nanopowders* **5**
[21] Sharif M K, Khan M A, Hussain A, Iqbal F, Shakir I, Murtaza G, . . . and Warsi M F 2016. Synthesis and characterization of Zr and Mg doped $BiFeO_3$ nanocrystalline multiferroics via micro emulsion route. *Journal of Alloys and Compounds* **667** 329-340
[22] Chen Q, De Marco N, Yang Y, Song T-B, Chen C-C, Zhao H, . . . and Yang Y 2015. Under the spotlight: The organic–inorganic hybrid halide perovskite for optoelectronic applications. *Nano Today* **10(3)** 355-396
[23] Hosseini S, Sarsari I A, Kameli P, and Salamati H 2015. Effect of Ag doping on structural, optical, and photocatalytic properties of ZnO nanoparticles. *Journal of Alloys and Compounds* **640** 408-415
[24] Cheng Z, Wang X-L, Du Y, and Dou S 2010. A Way to Enhance the Magnetic Moment of Multiferroic Bismuth Ferrite. *Journal of Physics D: Applied Physics* **43** 242001
[25] Fu C, Long X, Cai W, Chen G, and Deng X 2014. Structural and Magnetic Properties of Bismuth Ferrite Nanopowders Prepared via Sol-Gel Method. *Ferroelectrics* **460(1)** 157–161
[26] Kaur J, Bansal S, and Singhal S 2013. Photocatalytic degradation of methyl orange using ZnO nanopowders synthesized via thermal decomposition of oxalate precursor method. *Physica B: Condensed Matter* **416**
[27] Singhal S, Chawla A K, Gupta H O, and Chandra R 2009. Influence of Cobalt Doping on the Physical Properties of $Zn_{0.9}Cd_{0.1}S$ Nanoparticles. *Nanoscale Research Letters* **5(2)** 323-331
[28] Ferrara M, and Bengisu M 2014. Materials that Change Color for Intelligent Design. *Materials that Change Color* 9-60
[29] Sundararajan M, John Kennedy L, Nithya P, Judith Vijaya J, and Bououdina M 2017. Visible light driven photocatalytic degradation of rhodamine B using Mg doped cobalt ferrite spinel nanoparticles synthesized by microwave combustion method. *Journal of Physics and Chemistry of Solids* **108(Supplement C)** 61-75
[30] Dong H, Zeng G, Tang L, Fan C, Zhang C, He X, and He Y 2015. An overview on limitations of

TiO_2-based particles for photocatalytic degradation of organic pollutants and the corresponding countermeasures. *Water Research* **79** 128-146

6. Acknowledgement

We would like to thank Laser Centre and Faculty of Science, Universiti Teknologi Malaysia (UTM) for providing research facilities. This research work has supported by grant UTM Tier 2 RUG, R.J130000.2654.17J39